Article

Data-Driven Optimized Artificial Neural Network Technique for Prediction of Flyrock Induced by Boulder Blasting

Xianan Wang [1], **Shahab Hosseini** [2,*], **Danial Jahed Armaghani** [3,*] and **Edy Tonnizam Mohamad** [3]

1   School of Civil and Architectural Engineering, Anyang Institute of Technology, Anyang 455000, China;
    20160424@ayit.edu.cn
2   Faculty of Engineering, Tarbiat Modares University, Tehran 14115-175, Iran
3   Centre of Tropical Geoengineering (GEOTROPIK), Institute of Smart Infrastructure and Innovative
    Engineering (ISIIC), Faculty of Civil Engineering, Universiti Teknologi Malaysia,
    Johor Bahru 81310, Malaysia; edy@utm.my
*   Correspondence: h.seyyedshahab@modares.ac.ir (S.H.); jadanial@utm.my (D.J.A.)

Abstract: One of the most undesirable consequences induced by blasting in open-pit mines and civil activities is flyrock. Furthermore, the production of oversize boulders creates many problems for the continuation of the work and usually imposes additional costs on the project. In this way, the breakage of oversize boulders is associated with throwing small fragments particles at high speed, which can lead to serious risks to human resources and infrastructures. Hence, the accurate prediction of flyrock induced by boulder blasting is crucial to avoid possible consequences and its' environmental side effects. This study attempts to develop an optimized artificial neural network (ANN) by particle swarm optimization (PSO) and jellyfish search algorithm (JSA) to construct the hybrid models for anticipating flyrock distance resulting in boulder blasting in a quarry mine. The PSO and JSA algorithms were used to determine the optimum values of neurons' weight and biases connected to neurons. In this regard, a database involving 65 monitored boulders blasting for recording flyrock distance was collected that comprises six influential parameters on flyrock distance, i.e., hole depth, burden, hole angle, charge weight, stemming, and powder factor and one target parameter, i.e., flyrock distance. The ten various models of ANN, PSO–ANN, and JSA–ANN were established for estimating flyrock distance, and their results were investigated by applying three evaluation indices of coefficient of determination (R^2), root mean square error (RMSE) and value accounted for (VAF). The results of the calculation of evaluation indicators revealed that R^2, values of (0.957, 0.972 and 0.995) and (0.945, 0.954 and 0.989) were determined to train and test of proposed predictive models, respectively. The yielded results denoted that although ANN model is capable of anticipating flyrock distance, the hybrid PSO–ANN and JSA–ANN models can anticipate flyrock distance with more accuracy. Furthermore, the performance and accuracy level of the JSA–ANN predictive model can estimate better compared to ANN and PSO–ANN models. Therefore, the JSA–ANN model is identified as the superior predictive model in estimating flyrock distance induced from boulder blasting. In the final, a sensitivity analysis was conducted to determine the most influential parameters in flyrock distance, and the results showed that charge weight, powder factor, and hole angle have a high impact on flyrock changes.

Keywords: flyrock; blasting; soft computing; ANN; jellyfish research algorithm; particle swarm

MSC: 68T20; 68T01

1. Introduction

Blasting works typically involve applying the intensity of an explosion to rock masses in order to break them apart and displace them. Some of the explosives' strength is employed in these operations to accomplish the targeted objectives, and a considerable amount of them is wasted [1]. In addition, blasting energies have an effect on a wide

variety of places in the surrounding blasting area, the majority of which are undesired and ruinous. The wasted blasting energy is applied to release undesirable environmental and destructive side effects such as flyrock, dust emission, toxic gas pollution, ground vibration, backbreaks, toe problems, boulders, etc. [2–5].

The term "fly rock" describes the egregious fragmentation that produces under random status at the place beyond the intended explosion-safe boundary [6]. This undesirable problem of blasting poses a significant risk, particularly when machinery and buildings are positioned near the locations of the blasting sites [7]. The boulders that are formed as a result of blasting are referred to as "oversize boulders" in the mining industry. Only specific transportation machines and crusher tools can manage the large fragmentation (oversize boulders) in any way, including loading, transporting, or loading operations. When viewed from a more pragmatic perspective, oversize boulders are considered fragmented sizes that must undergo repeated blasting and breakage to be processed further—this process is named secondary blasting. Due to the difference in types of transportation and crushing machinery utilized varies from one activity to the other, it is difficult and impractical to assign a dimension or range of measurements of the oversize boulders [8]. The appropriate rock particles to standard and optimum equipment's loading and hauling cause enhance the productivity and effectiveness of the transporting machines and crushers and reduce the practical costs of processing. Furthermore, the best import rock sizes into a crusher are the size that decrements its maximum efficiency, power consumption, and the amount of wear and tear due to crushing rocks.

Oversize boulders may cause a variety of effects on the efficiency of operational mining processes, including the necessity for supplemental time required for separating chunks, inadequate loading works, secondary blasting, the imposition of additional costs, additional wear on transportation machines and their possible destruction, and incrementing in the amortization of the trucks, shovels and crushes. The formation of oversize boulders in mine and quarry sites will actually occur based on different factors, which can be divided into the following four categories (Figure 1): (1) geologically associated circumstances; (2) blasting design pattern parameters; (3) type and characteristics of explosive; and (4) human-related factors [9].
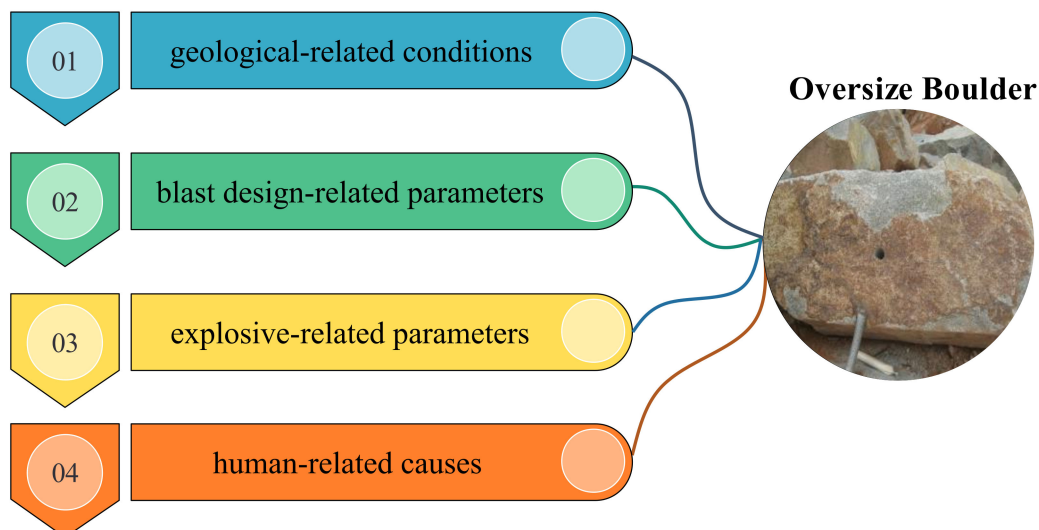
Figure 1. Factors to produce blast-induced oversize boulders.

One of the most significant parameters that affect the production of oversized boulders is the descriptive geology situation. Geological conditions play a crucial role in the generation of blast-induced oversize boulders, not just near the blasting faces but additionally from inside the shot. Nevertheless, controlling geological conditions during designing and performing blasting operations is impossible because it is classified as a group of uncon-

trollable parameters [10]. Blasting pattern design parameters are an additional category of important parameters that are used for producing oversize boulders. These parameters should be adjusted optimally to generate appropriate fragment size distribution.

Some of the blasting pattern design factors, including stemming, hole depth, hole diameter, burden, and spacing, are illustrated in Figure 2, and categorized in the controllable parameters of blasting rounds and can be determined by the designer and mine engineers to obtain optimum rock fragmentation.
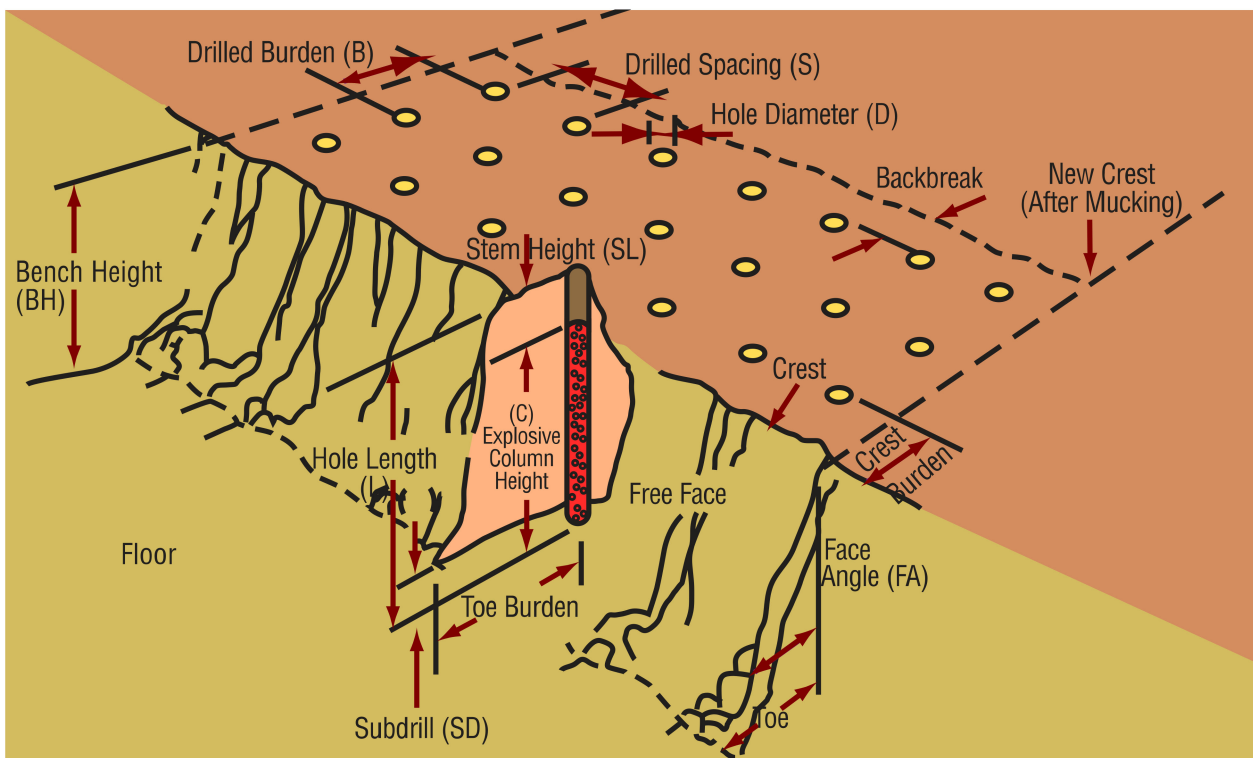
Figure 2. A view of blasting bench and pattern design parameters.

The characteristics of explosives are discussed in the third category. The widest explosives used in mine blasting are dynamite, water gel, and ANFO, which have different densities, resistivities, and specific charges. Therefore, these parameters also have considerable effects on oversize boulders due to bench blasting [9]. Mistakes that were caused by human intervention in the designing and carrying out of blasting activities are other affecting parameters on oversize boulders. The blasting team constantly maintains control over the performance of the blasting designs and ensures that they are finished [11].

Over the past several decades, there have been numerous experimental and empirical systems proposed with the intention of forecasting the particle size distribution and flyrock produced by bench blasting [11–13]. On the other hand, because of the present complicated circumstances of the blast design process, the findings of the proposed experimental systems were not satisfactory [14]. As a result, presenting a unique empirical model for the purpose of predicting flyrock and rock fragmentation is unacceptable and unexpected [15]. In addition to empirical approaches, many studies developed statistical models and formulas to determine the flyrock and fragment rock sizes (see Table 1). Nonetheless, using statistically based methods to solve a highly non-linear issue such as flyrock and rock fragmentation can be a challenging and difficult endeavor. Many attempts are conducted to solve engineering problems by using artificial intelligence and soft computing techniques [16–25]. Therefore, the application of intelligent machine learning, such as artificial intelligence (AI) and soft computing (SC), could have relevance and benefit when attempting to solve issues related to this type. These methods have successfully been applied to

effectively apply in a variety of disciplines of engineering, and the conclusions drawn from those applications have been advocated as solutions to real-world issues (see Table 1). In the last decade, numerous attempts have been conducted to model blast-induced flyrock phenomena in mines and predict its' distance utilizing artificial intelligence techniques (Table 1).

Table 1. Some studies conducted in the field of flyrock prediction.

Reference	Year	Inputs	AI Algorithm
[1]	1975	HD	Empirical
[26]	1981	HD, SC	Empirical
[2]	1988	ST/B	Empirical
[27]	2005	B, ST, HD	Empirical
[15]	2009	HD, Fs	Empirical
[28]	2010	HD, ST, BS, SD, PF, Qmax, N, RD	ANN
[7]	2011	B, S, HD, ST, SD, PF, Qmax, RD	FIS, SM
[8]	2011	B, S, HD, ST, PF, Qmax, BI, RMR	ANN
[9]	2011	d, B, HD, ST, BS, SD, PF, Qmax, BI	ANN
[29]	2012	B, S, HD, ST, SD, PF, Qmax, RMR	ANN-GA
[10]	2012	PF, HD, SD, S, d, B, ST	ANN, SVM
[30]	2012	B, S, ST, HD, HD, SC, Q	Empirical
[31]	2013	HD, S, B, d, Qmax	ANN
[32]	2013	HD, S, B, ST, PF, SD	SVM
[13]	2014	B, S, CPM, Q, σ_c, RQD	MVRA
[14]	2014	PF, S, HD, ST, B, Qmax	FIS, ANN
[33]	2015	d, B, S, HD, Q, CPM, σ_c, RQD	ANN, ANFIS
[34]	2016	BDF, EDF, RMR	Empirical
[35]	2016	B, S, CPM, PF, σ_c, RQD	MVRA, BPNN
[36]	2018	B/S, H/B, SD, PF, Qmax RD	LS-SVM, SVR
[37]	2019	B/d, S/B, ST/B, H/B, PF, Xb	MDA
[38]	2020	B, S, ST, PF RD	ELM
[39]	2020	B, S/B, ST/B, H/B, d, B/d, PF, Qmax, VoD RMR, BI	FRES
[6]	2022	B, S, ST, PF, Q	Z-FCM-ANN
[3]	2022	N, HD, B, S, ST, BRH, PF, Q	ANN
[40]	2022	ST, Q, PF	ANN
[41]	2022	d, HD, S, PF, B/S, ST, Qmax	ANFIS, HGSO-ANFIS
[42]	2023	HD, S, B, ST, PF	DT, XGBoost, AdaBoost

According to the abovementioned literature and Table 1, although a precise and smart model for estimating oversize boulders and flyrock is of relevance in mining operations, there is no research that considers the resulting flyrock from boulder blasting. Hence, this study focuses on structuring a smart system for the accurate prediction of flyrock after boulder blasting. The phase of proposing a predictive model is organized using the present optimized multi-layer perception neural network by three optimization algorithms, i.e., PSO and jellyfish search algorithm (JSA). The method employed in this research to anticipate flyrock after oversize boulder blasting is transferable to the solution of various unwelcome problems that can arise from blasting operations in mine and quarry sites. The remainder of the paper is organized as follows: Section 2 provides Methods and Materials. The description of the case study and analysis of the required data are presented in Section 3. The model development and performance of developed models in this study are presented in Section 4. Section 5 addresses the results and discussions. Finally, the obtained results are concluded in Section 6.

2. Methods and Materials

2.1. Jellyfish Search

Chou and Truong [43] presented an Artificial Jellyfish Search (JSA) algorithm in 2021 by modeling it after the predatory procedures carried out by jellyfish, which comprises

three involvement of behaviors: (i) jellyfish generally observe a single regulating point, which may be the ocean current or the movement of individuals within the group, as well as a temporal control mechanism, (ii) jellyfish are more interested in locations in which there is a greater quantity of food available, and (iii) the quantity of food is allotted, and the fitness function for it is calculated in accordance with the allocation.

2.1.1. Population Initialization

The initializing of the individuals in JSA is performed using the information on a logical diagram [44], which removes the adverse impacts of randomly generated initial values commonly approved by conventional metaheuristics, such as a minimal convergence speed and a local optimum that can present a fall hazard as a consequence of an absence of the jellyfish variety. The following is an expression of the JSA-based rational diagram [43]:

$$X_{i+1} = \vartheta X_i (1 - X_i), \quad 0 \le X_0 \le 1 \tag{1}$$

in which X_i signifies the chaotic position values of the ith jellyfish, X_0 indicates the initially generated jellyfish, and the ϑ is equal to 4.0 [43].

2.1.2. Ocean Current

Ocean currents that include significant quantities of nutrients attract jellyfish to a location and update their position based on the trend that ocean currents are moving in. The following equation can serve as a model for it:

$$X_i(t+1) = X_i(t) + rand(0,1) \times (X^* - \beta \times rand(0,1) \times \mu) \tag{2}$$

where X^* indicates the populations of jellyfish optimal position, μ denotes the average location of the jellyfish swarm, and β stands for the distribution-related factor, which number is fixed to 3.

2.1.3. Jellyfish Swarm

There are two categories of jellyfish motion in swarms: passive and active motions. Throughout repetitions, the position of a particular jellyfish is updated as follows:

$$X_i(t+1) = X_i(t) + \gamma \times rand(0,1) \times (U_b - L_b) \tag{3}$$

where Ub and Lb stand the upper and lower bounds of the search area, and c refers to the motion-related factor, which is fixed at 0.1.

The following equation simulates the jellyfish in the swarm's active motion:

$$X_i(t+1) = X_i(t) + rand(0,1) \times \overrightarrow{direction} \tag{4}$$

A jellyfish swarm perpetually proceeds in the path in which there is a greater supply of food, which displays the direction of the motions of jellyfish within the population. The following objective function (OF) equation is used to determine the motions direction of individual jellyfish:

$$\overrightarrow{direction} = \begin{cases} if \ f(X_j) \ge f(X_i) & X_j(t) - X_i(t) \\ if \ f(X_j) < f(X_i) & X_i(t) - X_j(t) \end{cases} \tag{5}$$

where f is the OF related to location X.

2.1.4. Time Control Mechanism

The timing control scheme in JSA has been modified such that it may be used to direct the motion of jellyfish in response to ocean currents and among swarms of jellyfish. The

execution of JSA is heavily reliant on the timing regulating function *c(t)*, which arbitrarily vacillates between the range of 0–1 and may be represented as follows:

$$c(t) = \left| \left(1 - \frac{k}{k_{max}} \right) \times (2 \times rand(0,1) - 1) \right| \tag{6}$$

where *k* represents the total number of repetitions, k_{max} signifies the maximum number of iterations, and Figure 3 presents the flowchart of JSA. The pseudocode of the jellyfish search algorithm is shown in Figure 4.
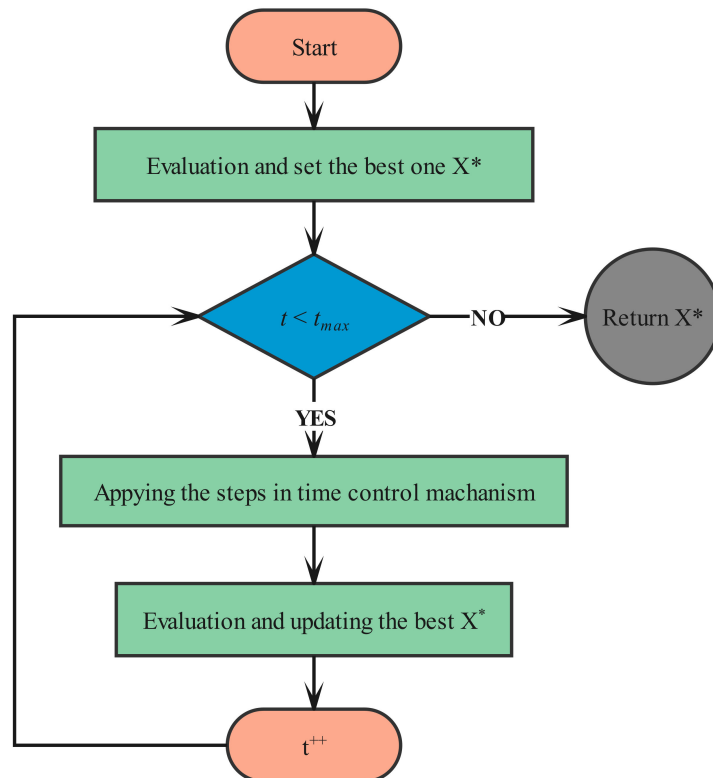
Figure 3. Algorithmic flowchart of the jellyfish search algorithm.

2.2. Particle Swarm Optimization

Particle swarm optimization, abbreviated as PSO, is a metaheuristic algorithm that was first introduced by Kennedy and Eberhart [45]. The accumulated behavior of particles served as motivation for the development of PSO. PSO has a significantly higher learning performance and uses much less memory than the other algorithms, such as the genetic algorithm. These are just two of the many benefits of adopting PSO. This algorithm uses a population of particles to search for the best personal (p_{best}) and best global (g_{best}) coordinates in order to determine the optimal location. In other words, throughout every repetition of the process, the particles advance in the direction of discovering the optimal places. The following are the formulas that can be used to calculate the speed and location of the particles:

$$V_{new} = w \times V + C_1 \cdot r_1(p_{best} - X) + C_2 \cdot r_2(g_{best} - X) \tag{7}$$

$$X_{new} = X + V_{new} \tag{8}$$

in which *V* is the first velocity, *X* denotes the particles' positions, C_1 and C_2 indicate the constants related to positive acceleration, V_{new} signifies the new velocity, X_{new} represents the location of particles, *w* is the inertial weight, and r_1 and r_2 stand the ran-

dom numbers in the range of (0, 1). The diagram and flowchart of PSO are illustrated in Figures 5 and 6, respectively.

Input:	n_{pop} : Population size	Dim: number of dimensions of search space
	$Max_{\_iter}$: Maximum number of iterations	UB: Upper bound on search space
		LB: Lower bound on search space
		f($\mathbf{X}$): Objective function

Initialize population of jellyfish $\mathbf{X}_i$ (i=1, 2,.., n_{pop}) using logistic chaotic map
Calculate the quantity of food at each $\mathbf{X}_i$ as f($\mathbf{X}_i$)
Find the jellyfish at the location currently with the most food ($\mathbf{X}^*$)
For t = 1 to $Max_{\_iter}$ **do**
  For i = 1 to n_{pop} **do**
    Calculate the time control c(t) using
$$c(t) = \left| \left(1 - \frac{t}{Maxiter}\right) \times (2 \times rand(0,1) - 1) \right|$$
    If c(t)≥ C_o:
    Jellyfish follows ocean current
      Determine ocean current
      $\overrightarrow{\mathbf{trend}} = \mathbf{X}^* - \beta \times rand(0,1) \times \boldsymbol{\mu}$
      New location of jellyfish is given by
      $\mathbf{X}_i(t + 1) = \mathbf{X}_i(t) + rand(0, 1) \times \overrightarrow{\mathbf{trend}}$
    Else
    Jellyfish moves inside a swarm
      If rand(0,1)>(1-c(t))
      Jellyfish exhibits type A motion (passive motion)
      $\mathbf{X}_i(t + 1) = \mathbf{X}_i(t) + \gamma \times rand(0,1) \times (\mathbf{Ub} - \mathbf{Lb})$
    Else
    Jellyfish exhibits type B motion (active motion)
      Determine direction of jellyfish using
      $\overrightarrow{\mathbf{Direction}} = \begin{cases} \mathbf{X}_j(t) - \mathbf{X}_i(t) & \text{if } f(\mathbf{X}_i) \geq f(\mathbf{X}_j) \\ \mathbf{X}_i(t) - \mathbf{X}_j(t) & \text{if } f(\mathbf{X}_i) < f(\mathbf{X}_j) \end{cases}$
      $\overrightarrow{\mathbf{step}} = rand(0,1) \times \overrightarrow{\mathbf{Direction}}$
      $\mathbf{X}_i(t + 1) = \mathbf{X}_i(t) + \overrightarrow{\mathbf{step}}$
    End if
  End for
  Check whether boundary conditions are satisfied and calculate quantity of food at new location
  Calculate quantity of food at new location f(X_i)
End for

| **Output**: | The best solution so far |

Figure 4. Pseudocode of the jellyfish search algorithm.
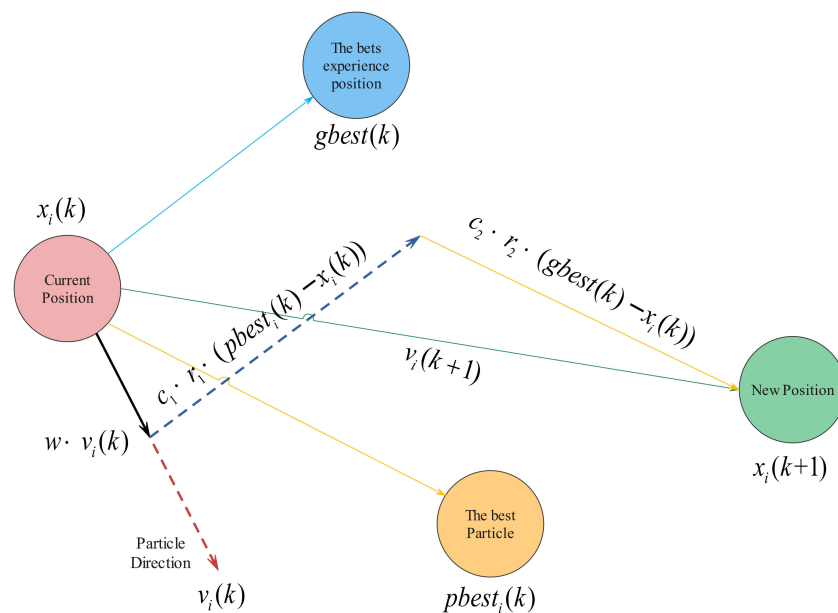
Figure 5. The diagram of the PSO algorithm.
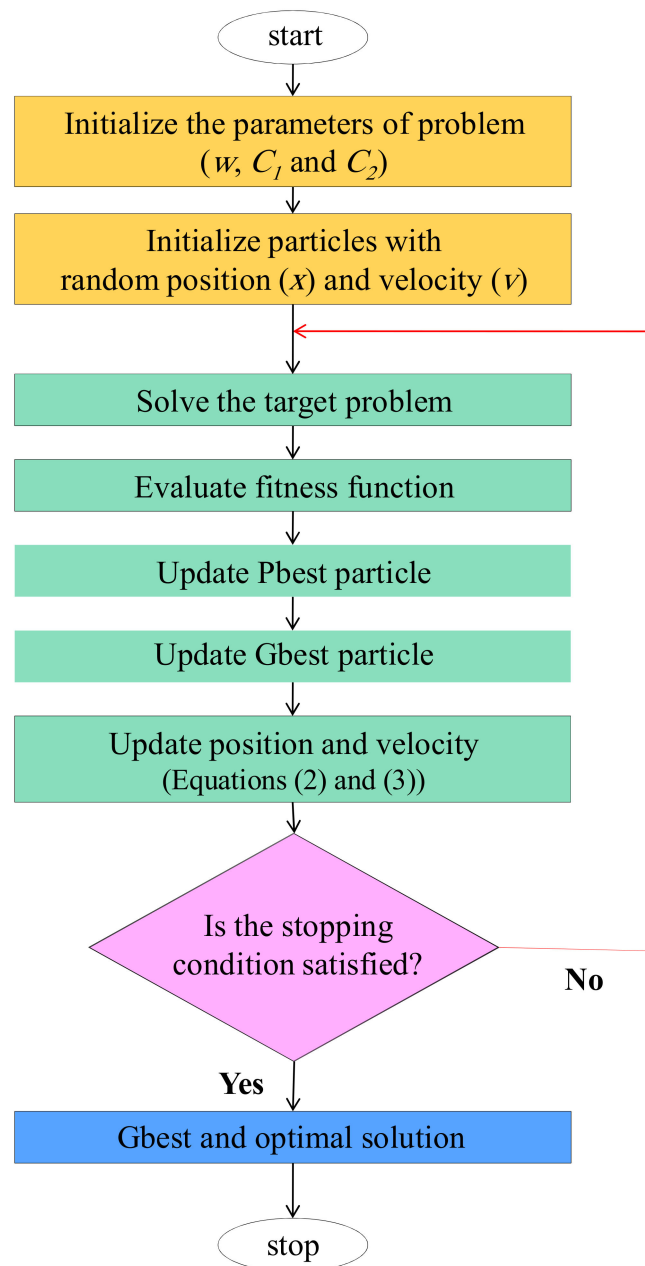
Figure 6. The flowchart of the PSO algorithm.

2.3. Artificial Neural Network

Artificial neural networks (ANN) originate from the structure of human brains in information processing. In the human brain, first, the information is imported and then proceed by neurons. Finally, the output information is output to execute commands. In the processing step, a training process is performed by neurons to obtain accurate and correct information. This process is also conducted for neural networks. ANNs comprise the main three layers involving inputs, output(s), and hidden layers. The main role of each layer is to keep the neurons (binding components) together in each layer and connect them through the weights. The neurons pass the information received from the input source to the next level (layers) [46]. The available data are transmitted from the input neurons to the hidden neurons and, subsequently, to the output neurons (last layer). This data transfer from one layer to another is associated with oscillation (strengthening or weakening), which is controlled by the weights in each layer. However, the main core of neural network processing is the neural computations performed in each layer; meanwhile, in the first

step, the imported data into the system is weighted. Then, the linear or sigmoid transfer function is utilized to pass data to the first hidden layer. Finally, the new data generated in the hidden layer are transferred to the output layer based on a similarly expressed process. It is noteworthy that the important components in the ANNs are the neurons' number in layers because the neurons affect the network performances [47]. Based on this, the number of input and output neurons is equal to the number of imported input and outputs to the system, respectively. However, the hidden neurons are determined according to a trial–error procedure. In the mentioned explanation, the data processing is conducted based on the available training algorithms, in which the feedforward-backpropagation (BP) algorithm is widely applied in network training because of its accuracy and speed.

It should be noted that the weighting of neurons during transmitting data is performed randomly; the random weights and biases are generated and modified in the training step. The design of the network structure and the calculation of the appropriate weight are the two primary components that constitute the ANN modeling process. The BP training method applies adjustments to the network weights in order to minimize error levels by using those values. The values that are acquired at each step are compared with the values that are wanted for the output at the end of the process. In the event that the errors are undesirable, the procedure should be repeated to obtain the required values and bring the system error to an acceptable level.

2.4. Hybrid System

Several studies have been conducted in the field of engineering applications to improve the capabilities of ANNs models by using optimization techniques (Table 1). It is possible that the ANN model can also provide unacceptable predictions due to the fact that BP is not really that efficient at locating the precise global minimum. However, the ANN technique has a greater propensity to get stuck in local minima, whereas optimization algorithms, by adjusting the weight and bias of ANNs, can overcome this problem. In the current research, a JSA as a novel metaheuristic algorithm is combined with the ANN, named the JSA–ANN hybrid system, to predict flyrock distance from boulder blasting. Then, the prediction result of JSA–ANN was compared to the PSO algorithm. The hybrid systems search a global minimum, and then ANN selects the method that has the potential to provide the highest accuracy.

3. Case Study and Data Analysis

For access to the required datasets, the Ulu Tiram quarry mine was considered, which is explored in the Johor site in Malaysia. The geographical location of the Ulu Tiram quarry mine is at a latitude of $1°36'41''$ N and a longitude of $103°49'0''$ E. The main ore extraction in this mine is granite, with rock strength ranging from 50–90 MPa. The production rate of Ulu Tiram quarry mine for each month is 15,000–35,000 tons, which is supplied through the implementation of blasting operations. The boulder production-induced mine blasting was regarded as one of the most significant ecological challenges in the aforementioned locations. Normally, after several blasting (i.e., primary blasting), there is a need to blast the boulders produced by these primary blasts. The site's regular hauling and crushing equipment are unable to manage the enormous boulder in any way, including loading, transporting, or handling it. From a more pragmatic standpoint, an oversize boulder can be thought of as a fragment size that must first be subjected to secondary blasting and fracture before any further processing can take place. It is not possible to assign a size or set of dimensions to the oversize boulder since the method of loading, transferring, and crushing the rock varies from one operation to the next. In the mentioned quarry, a total number of 20 boulders with a volume ranging between 2.1–3.8 m^3 were investigated, and the relevant information, together with their flyrock values, were measured.

In total, sixty-five blast datasets were gathered, with each containing information on the hole diameter, hole depth, burden, hole angle, charge weight, stemming, powder factor, and boulder distance as an output. Ammonium nitrate and fuel oil (ANFO) were charged

as explosives in blasting rounds. The maximum and minimum blast-hole diameters of 2.95 and 5.9 inches, respectively, were used in various procedures. The effective parameters of boulder blasting and corresponding ranges are reported in Table 2. In addition, the distribution plot of effective parameters listed in Table 2 is depicted in Figure 7.

Table 2. The range of effective parameters on flyrock distance.

Input							Output
Parameters	Hole Depth	Burden	Hole Angle	Charge Weight	Stemming	Powder Factor	Flyrock Distance
Sign	HD	B	HA	CW	St	PF	Flyrock
Unit	(cm)	(cm)	(°)	(kg)	(cm)	(kg/m^3)	(m)
Min	71	57	22	2.7	31	0.6	157
Average	86.91	77.18	27.46	3.41	39.80	0.79	227.66
Max	101	96	33	4.3	49	1.01	300
Standard Deviation	7.11	10.63	2.95	0.40	5.41	0.10	37.54
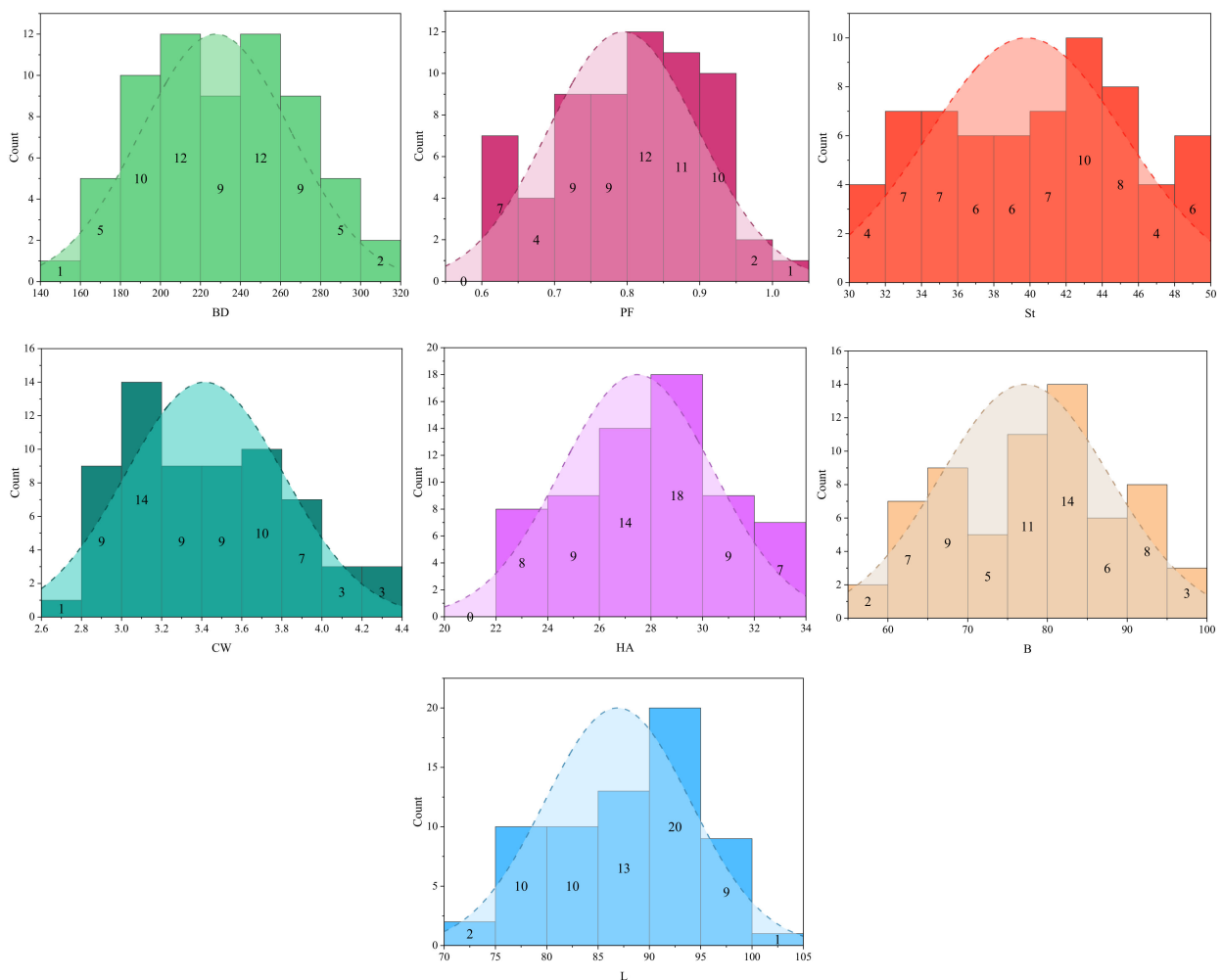
Figure 7. The histogram plot of effective parameters on flyrock distance.

Two video cameras were installed to capture the maximum distance of fragmented boulder pieces. The prepared benched for performing blasting rounds were colored to indicate the spaces between blasted boulders. Utilizing the aforementioned cameras, the

pieces of boulders could be distinguished after the explosion. The maximum distance of fragmented boulder pieces was then determined to be the horizontal separation of pieces at their greatest. It is noteworthy that the data collected in this research have not been used in the research literature before, and for the first time in this research, the prediction of the maximum distance of fragmented boulder pieces is addressed. Figure 8 shows the production of a large number of boulders that require secondary blasting to be fragmented into portable sizes. Furthermore, the drilling of holes with a diameter of 8.9 cm in boulders is shown in Figure 9.

Figure 8. Oversize boulders in the case study.

Figure 9. The drilled hole in the oversize boulder for charging and blasting operation.

4. Model Development

In this paper, the modeling and estimation of flyrock distance due to oversize boulder blasting were performed by the ANN model and hybrid systems of PSO–ANN and JSA–ANN. To do this, the four main steps were considered; (1) the available 65 datasets that were collected in a quarry mine in Malaysia were randomly classified into two phases training data (80% of whole data, 52 datasets) and testing data (20% of whole data, 13 datasets). (2 All of the data, including six influential parameters and flyrock data, were converted to normalized values in the range of $[-1,1]$ utilizing the following equation [5]:

$$x_n = \frac{x_i - x_{min}}{x_{max} - x_{min}} \tag{9}$$

in which x_n, x_i, x_{min}, and x_{max} are the normalized values, measured data, and minimum and maximum of datasets, respectively. (3) The capabilities of the developed models were assessed using three evaluation metrics, including R^2, RMSE, and VAF, which can be calculated as follows [48]:

$$R^2 = 1 - \left(\frac{\sum\limits_{i=1}^{n} (O_i - P_i)^2}{\sum\limits_{i=1}^{n} (P_i - \overline{P}_i)^2} \right) \tag{10}$$

$$RMSE = \sqrt{\frac{1}{n} \sum\limits_{i=1}^{n} (O_i - P_i)^2} \tag{11}$$

$$VAF = 100 \cdot \left(1 - \frac{var(O_i - P_i)}{var(O_i)} \right) \tag{12}$$

where *Oi* and *Pi* indicate actual and anticipated values, respectively; is the average of the anticipated amounts, and n stands the number of data. (4) The determined statistical metrics were rated by a rating system proposed by Zorlu et al. [49], and a color intensity system was used to validate the results of the rating system.

4.1. ANN

In this study, the examination of flyrock distance was the main emphasis. In order to obtain the structure that has the highest efficiency and is capable of forecasting flyrock distance accurately and to the best degree of accuracy, a variety of network models were developed using a variety of hidden neuron sizes and transfer functions. To pass the data from the structured layer to the next layer in an architecture, transfer functions including "LOGSIGMOID", "TANSIGMOID", and "PURELIN" were used, along with a variety of training techniques, including, among others, "trainlm", "trainoss", and "traingdx". This evaluation was the assignment that was provided to the rating approach that was developed by Zorlu et al., and the R^2 and RMSE metrics were the metrics utilized in order to evaluate and choose the optimal architecture among the models that were run with high efficiency and precision. Using this method, the R^2 and RMSE values for the training and testing parts are calculated, and the scores for those quantities are determined. According to this ranking method, the ranking of the architecture is considered to be better when both the values of R^2 and VAF are larger and when the value of RMSE is smaller. Table 3 provides a rundown of the results of these computations in summary form.

It is important to highlight that the outcomes were evaluated using a technique known as color intensity rating (CIR), and the outcomes of both were examined. The CIR technique is a creative and quantitative tool for the problem of selecting the best ANN architecture. Within this approach, the architectures are each allocated a particular coloring (for example, blue), and the model that has a greater rating shows a higher color temperature.

Table 3. Different topology of ANN models in anticipating flyrock distance.

Model No.	Training			Testing			Training Rates			Testing Rates			Total Rate	Rank
	R^2	RMSE	VAF	R^2	RMSE	VAF	R^2	RMSE	VAF	R^2	RMSE	VAF		
1	0.880	13.106	65.783	0.848	11.256	83.126	1	1	1	1	1	1	6	10
2	0.938	8.194	98.110	0.931	7.509	92.166	7	9	9	9	9	9	52	2
3	0.916	10.542	97.858	0.894	10.303	89.412	3	2	8	6	2	8	29	6
4	0.940	8.235	93.983	0.879	9.821	86.232	9	8	4	3	5	4	33	5
5	**0.957**	**7.392**	**99.472**	**0.945**	**7.473**	**93.961**	**10**	**10**	**10**	**10**	**10**	**10**	**60**	**1**
6	0.917	9.934	91.989	0.864	10.027	85.595	4	4	3	2	4	3	20	9
7	0.905	10.215	93.983	0.882	9.055	88.025	2	3	4	4	7	6	26	8
8	0.919	9.559	96.439	0.909	8.771	88.772	5	6	7	7	8	7	40	3
9	0.939	8.544	91.989	0.885	10.130	85.588	8	7	2	5	3	2	27	7
10	0.928	9.611	93.983	0.928	9.699	87.771	6	5	4	8	6	5	34	4

The yellow color indicates the intensity of statistical metrics and their rates. Bold row indicates the best model.

On the other hand, the lower the rate of models, the lower their color temperature becomes, resulting in it becoming almost completely white. All of the numbers in Table 3 have been given the appropriate shading in light of these explanations and the procedure that has been presented. Table 3 presents ten distinct topologies, of which only one was deemed suitable for inclusion in the study as a candidate for the best ANN topology. Among the ten different topologies of ANN, only ANN5, which had received the highest rate possible, i.e., 60, was chosen to serve as the ideal architecture since it performed better than the other models. Furthermore, according to the mentioned scoring tool, the color that was designated to the ANN5 was used to have the maximum intensity. This indicates that all approaches are equivalent and provide very accurate results when selecting the best topology. Because of this, the ANN5 was chosen as the best available ANN model to predict flyrock distance. It has a structure of 6-4-10-1 (with two hidden layers), and the activation function of the input, hidden, and output layers are respectively "tansig", "tansig", and "purelin" type. Figure 10 shows the identified topology that was selected as well as the architecture that was produced by the toolbox of the MATLAB program.

As can be seen in Figure 10, the activation function of all layers was a sigmoid type. Figure 10 also demonstrates that a variable known as "bias" was used in all levels of the network, with the exception of the input layer. As a result, the prediction of the flyrock distance was carried out using the data collected from 65 boulder blasting, which were classified into train and test. The effectiveness of the ANN architectures that were constructed is compared in Table 3. The results indicated that the ANN model presents the R^2 values of 0.957 and 0.945 for the training and testing parts, respectively.

4.2. Hybrid Models

There are instances whenever the algorithms/models/techniques outperform other models when it involves estimating. Therefore, in this case, it could be advantageous for the modeling that was conducted better to be more heavily involved in the optimized hybrid models. The hybrid models are based on the concept that optimized models with more competence ought to have a greater influence on the results. This is accomplished by optimizing the weight and biases in the ANN structures. There are several ways to find these weights and biases. One of these suggestions is the use of metaheuristic optimization algorithms. This section addresses the development of hybrid models, i.e., PSO–ANN and JSA–ANN, for predicting flyrock-induced boulder blasting in open-pit mines. The controllable parameters applied in adjusting PSO and JSA are fixed in the optimization framework to yield the highest performance degree and accuracy level for flyrock estimation.
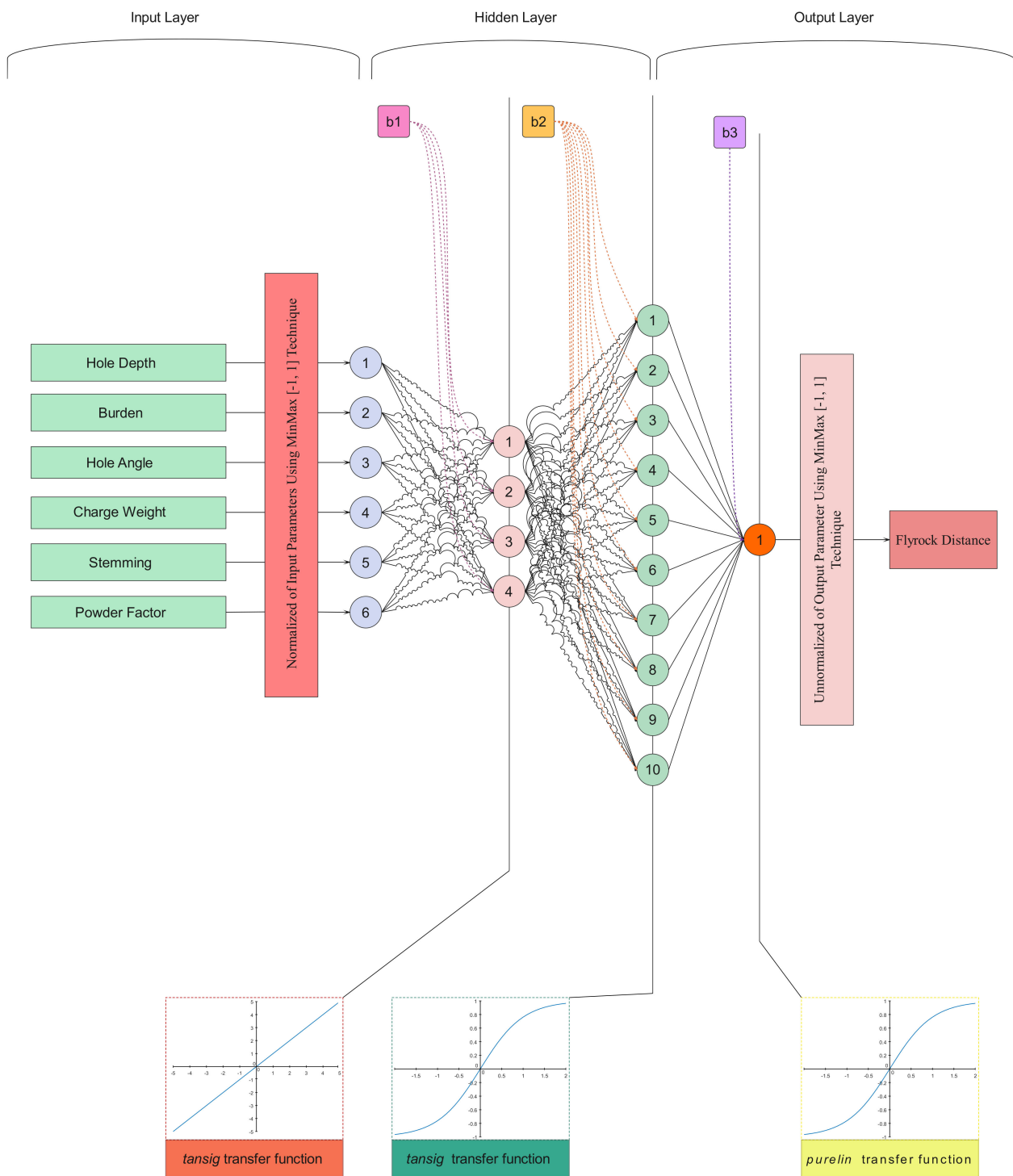
Figure 10. The designed ANN topology for predicting flyrock distance.

4.3. PSO–ANN

As aforementioned in PSO methodology, this metaheuristic algorithm is controlled by various parameters involving a number of particles, inertia weight, and velocity equation's coefficient that the iteration number managed error reduction. These parameters apply a considerable effect on the PSO. In this study, the inertia weight and velocity equation's coefficients are set at 2 and 0.25, respectively, due to the suggestion of previously conducted research [42] that obtained accurate prediction results. Hence, the inertia weight of 2 and the velocity equation's coefficient of 2.5 was employed in PSO–ANN modeling

process. Furthermore, the iteration number is considered as 1000 repetitions. Nevertheless, the parameter of the number of particles should be determined by the trial-and-error approach. Therefore, the swarm is defined as various populations, including 50 particles to 500 particles, and the RMSE function is used for evaluating the performance of PSO.

The obtained results of PSO in optimizing weights of neurons and biased values are depicted in Figure 11 and Table 4. Figure 11 illustrates the RMSE value obtained for each PSO swarm size. It can be found that the RMSE values of the PSO–ANN model converge for all swarm sizes in iteration 475. The different PSO–ANN systems were structured for anticipating flyrock distance based on various swarm sizes, as presented in Table 4, and then the best PSO–ANN system was chosen among the ten presented models. For better choosing, Zorlu's rating system was used, as shown in Table 4. The PSO–ANN with swarm sizes of 200 and a total rate of 41 was the superior model compared to other presented PSO–ANN models. The statistical metrics related to this model were the R^2 of (0.972 and 0.954), RMSE of (5.533 and 7.751), and VAF of (99.680 and 93.608), for the training and test phases, respectively.
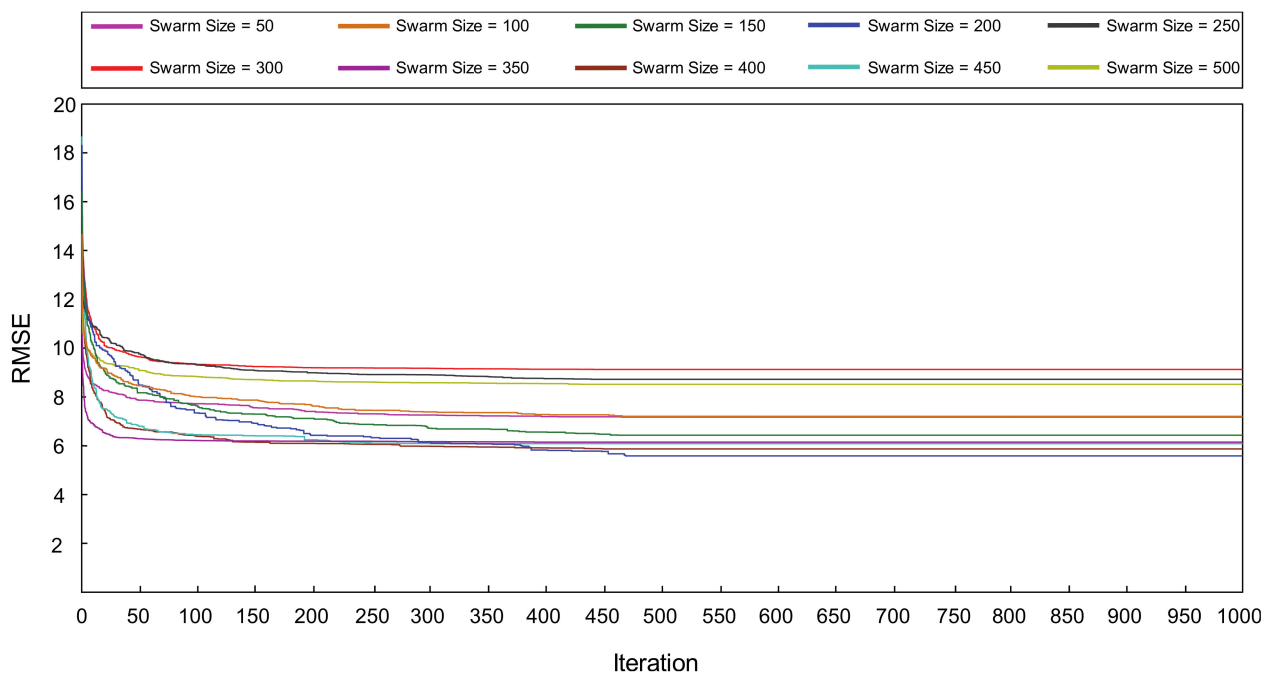
Figure 11. PSO–ANN models with different swarm sizes.

Table 4. Various swarm sizes of PSO in anticipating flyrock distance.

Model No.	Swarm Size	Training			Testing			Training Rates			Testing Rates			Total Rate	Rank
		R^2	RMSE	VAF	R^2	RMSE	VAF	R^2	RMSE	VAF	R^2	RMSE	VAF		
1	50	0.956	7.389	97.116	0.952	6.164	94.832	1	3	2	9	9	10	34	6
2	100	0.961	7.184	95.692	0.946	6.457	93.871	6	6	1	3	5	4	25	9
3	150	0.964	6.963	99.430	0.942	6.906	93.155	7	8	5	1	3	2	26	8
4	**200**	**0.972**	**5.533**	**99.680**	**0.954**	**7.751**	**93.608**	**10**	**10**	**7**	**10**	**1**	**3**	**41**	**1**
5	250	0.957	7.204	99.430	0.944	7.066	92.908	3	4	5	2	2	1	17	10
6	300	0.960	7.192	99.858	0.950	6.385	94.059	5	5	8	8	7	5	38	3
7	350	0.957	7.178	98.255	0.949	6.325	94.287	2	7	3	7	8	7	34	6
8	400	0.957	7.672	100.000	0.948	6.076	94.656	4	1	10	5	10	9	39	2
9	450	0.965	6.587	98.255	0.949	6.427	94.175	8	9	3	6	6	6	38	3
10	500	0.966	7.442	99.964	0.947	6.469	94.628	9	2	9	4	4	8	36	5

The green color indicates the intensity of statistical metrics and their rates. Bold row indicates the best model.

4.4. JSA–ANN

To obtain the optimum value of neuron weights and biases in the ANN architecture (6-4-10-1) that was designed in the previous section, the JAS algorithm was used. Nevertheless, the controllable parameters of JSA should first be adjusted and implemented to achieve the most accurate results. In this regard, the selected topology was employed in developing all hybrid systems. As described in the JSA methodology, the number of populations is considered a controllable parameter of JSA. To specify the best number of jellyfish, several JSA-ANN–ANN models with different populations, i.e., 25, 50, 75, 100, 125, 150, 175, 200, 225, and 250, were trained. The revealed results in Figure 12, the parametric investigation indicated that the number of jellyfish of 200 could achieve the best accuracy and higher system capacity.
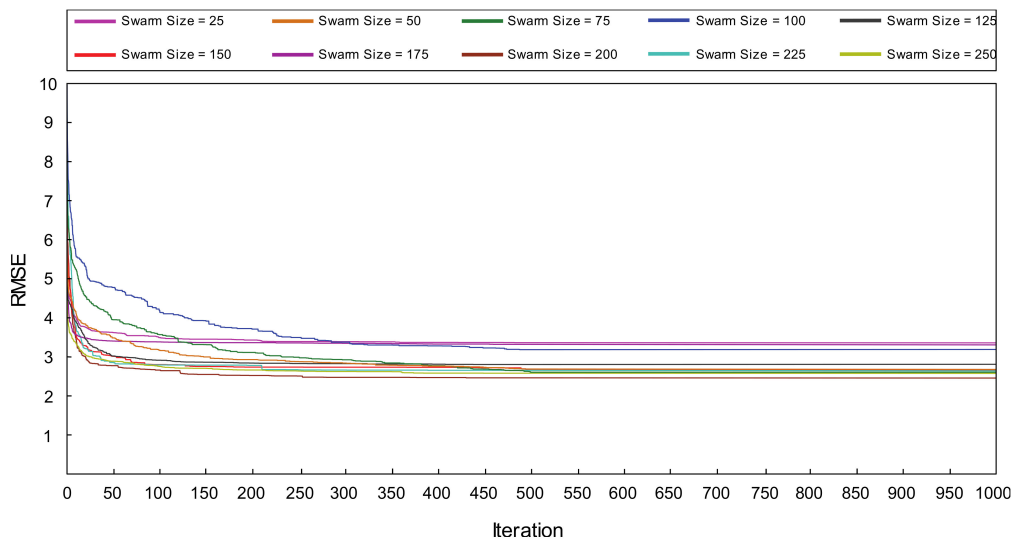
Figure 12. JAS–ANN models with different swarm sizes.

In the present research, the JSA optimization was implemented to identify the ANN model's optimum weights and biases. The JSA algorithm initializes by the originally created initial solution, similar to the existing evolutionary computing algorithms.

The JS algorithm searches the optimum values following the four main stages.

Stage 1. The initial population of the artificial jellyfish, X_i ($i = 1, 2, \ldots, n$), is generated using the chaotic map operation:

In the search space, the jellyfish serve as a model. The study's maximum iterations and the population size of the jellyfish are set at 1000 and 250, respectively.

Based on the trial-and-error procedure, beta and gamma have respective values of 4.5 and 0.09.

Stage 2. Finding the X^*:

In this study, the RMSE values are calculated to find the fitness function as shown in the following equation:

$$F_f = \sqrt{\left(\frac{\sum\limits_{i=1}^{n}\left(X_i^O - X_i^E\right)^2}{n_s}\right)} \tag{13}$$

in which X_i^O, X_i^E and n are the measured flyrock, obtained flyrock by the model, and a number of datasets, respectively. An artificial jellyfish with the lowest fitness function is given to the X^* by the algorithm.

Stage 3. Continue as follows until the maximum number of iterations has been reached:

Utilizing Equation (6), ascertain the time control function, $c(t)$.

Perform a local or global search for artificial jellyfish.

Examine the produced values and, when they do not fall inside the given ranges, replace them with new ones.

Considering the new values, and if the fitness function's value is the lowest, add it to *X**.

Here, the JSA method is used to find the weights that will be used to construct the basic models for the JSA–ANN model. Hence, a value between [0, 1] should be selected at random to preserve the $\sum_{i=1}^{n} W_i = 1$. The RMSE works as the cost function in this minimization process.

For selecting the best value for the number of jellyfish, the different JSA–ANN models with different populations were designed, and the results were evaluated based on the RMSE function, as illustrated in Figure 12. Based on Figure 12, RMSE changes are fixed after 500 iterations. Therefore, the JSA–ANN model with the number of jellyfish of 200, beta of 4.5 and gamma of 0.09 was constructed. The various generated results were compared and evaluated using the statistical metrics, i.e., R^2, RMSE, and VAF, as shown in Table 5. Similar to the evaluation of PSO–ANN, the developed JSA–ANN models were evaluated based on the rating system to choose the best JSA–ANN system with a high level of accuracy and acceptable performance prediction level.

Table 5. Different swarm sizes of JSA in anticipating flyrock distance.

Model No.	Swarm Size	Training			Testing			Training Rates			Testing Rates			Total Rate	Rank
		R^2	RMSE	VAF	R^2	RMSE	VAF	R^2	RMSE	VAF	R^2	RMSE	VAF		
1	25	0.988	3.788	99.964	0.990	4.368	98.706	1	1	8	9	2	9	30	6
2	50	0.988	3.629	98.718	0.971	4.197	96.525	2	2	4	2	4	3	17	9
3	75	0.991	3.425	97.721	0.978	4.261	96.460	6	4	3	5	3	2	23	8
4	100	0.990	3.299	99.110	0.979	3.573	97.597	4	5	5	6	6	5	31	5
5	125	0.990	3.214	99.430	0.976	3.453	97.649	5	6	7	4	7	6	35	4
6	150	0.989	3.587	97.116	0.964	4.796	96.313	3	3	2	1	1	1	11	10
7	175	0.995	2.791	99.964	0.992	3.282	98.664	9	9	8	10	8	8	52	2
8	**200**	0.995	2.449	100.000	0.990	2.602	98.832	10	10	10	8	10	10	58	1
9	225	0.992	3.095	99.110	0.983	3.101	98.300	8	8	5	7	9	7	44	3
10	250	0.992	3.150	96.439	0.975	3.700	97.298	7	7	1	3	5	4	27	7

The blue color indicates the intensity of statistical metrics and their rates. Bold row indicates the best model.

5. Results and Discussion

The purpose of the current research is to propose a precise model for modeling and predicting flyrock distance due to oversize boulder blasting in a quarry mine located in Malaysia. The most effective parameters were six numbers identified and imported into the modeling process. Based on the available data, the ANN model, as well as the two hybrid PSO–ANN and JSA–ANN systems, were developed to determine the superior predictive flyrock model between other proposed models. The obtained results relevant to the considered best models of ANN, PSO–ANN, and JSA–ANN based on R^2, RMSE, and VAF metrics in anticipating flyrock are shown in Table 6—these predictive models train well as a result of their high achievements in terms of the training data. The generated model achieves a high precision level among testing dataset indicates because it is well-developed.

Table 6. Results of the ANN and hybrid models in estimating flyrock distance.

Developed Model	Train			Test			Train Rating			Test Rating			Total Rate	Rank
	R^2	RMSE	VAF	R^2	RMSE	VAF	R^2	RMSE	VAF	R^2	RMSE	VAF		
ANN	0.957	7.392	91.989	0.945	7.473	93.961	1	1	1	1	2	2	8	3
PSO–ANN	0.972	5.533	99.680	0.954	7.751	93.608	2	2	2	2	1	1	10	2
JSA–ANN	0.995	2.791	99.964	0.989	2.896	98.872	3	3	3	3	3	3	18	1

Although all of the predictive models have the ability to predict flyrock, the JSA–ANN predictive model has the potential to deliver greater performance capabilities in terms of R^2 values throughout the training phase as well as the testing phase. According to these findings, the JSA–ANN model has the potential to achieve the lowest overall system error of all the models that have been applied. Figure 13 depicts the anticipated values for flyrock together with the measured values obtained from the application of the ANN, PSO–ANN, and JSA–ANN prediction models. The anticipated findings for both the training dataset and test phases are provided here in this figure. Based on this figure, despite the fact that all models have adequately performed the estimation of flyrock distance, the JSA–ANN model has the potential to establish itself as a novel hybrid system in this field. Table 7 illustrates the results that we have acquired about the effectiveness indicators of the developed model. The information presented in Table 7 shows a comparison between the prediction precision and capability level of our suggested method and that of a number of the most recent studies. According to the findings, the JSA–ANN model provides a higher performance ability in the modeling and prediction of flyrock than the other techniques.
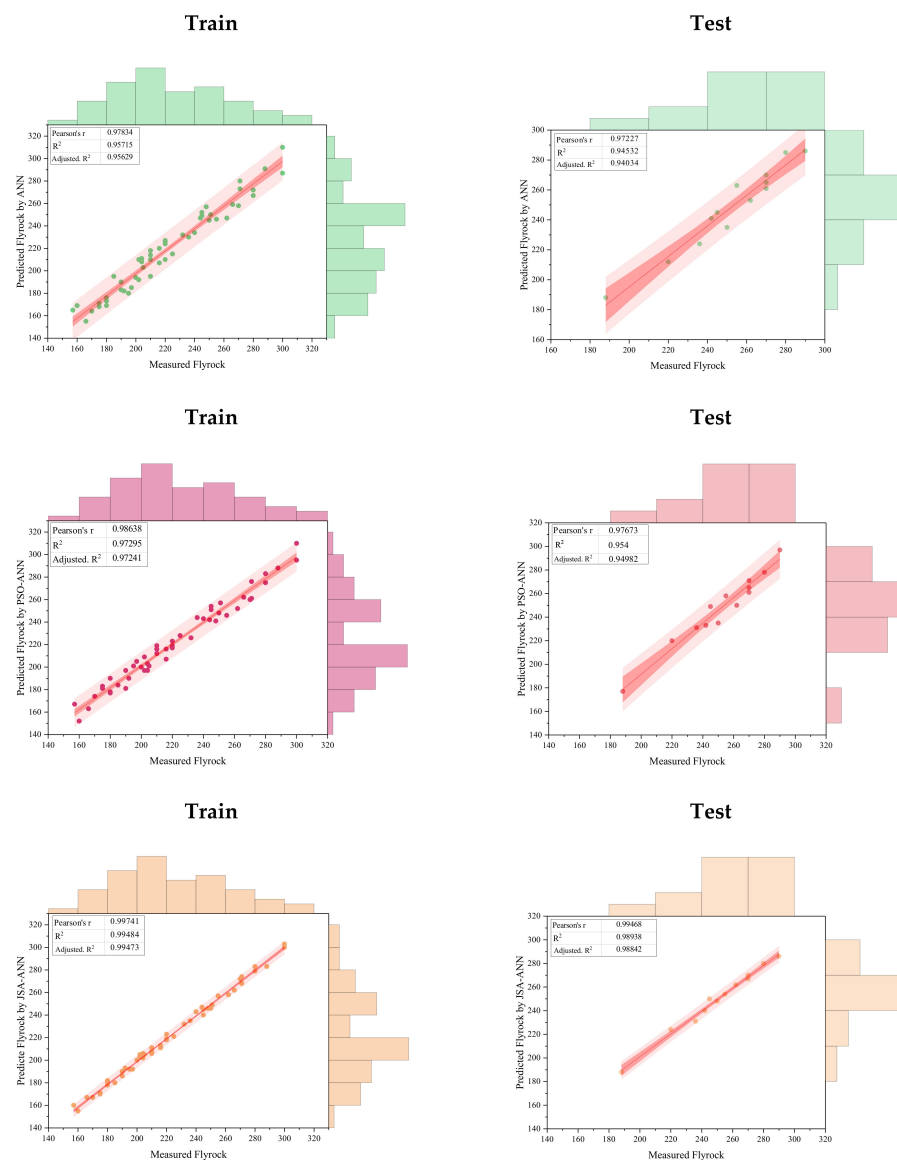
Figure 13. The results of developed models in predicting flyrock distance.

Table 7. Comparative analysis of the precision of our suggested method with that of other research.

Author	Year	Method	R^2
[38]	2020	Extreme Learning Machine	0.955
[39]	2020	FRES	0.981
[6]	2022	Z-FCM–ANN	0.991
[3]	2022	ANN	0.982
[41]	2022	HGSO-ANFIS	0.924
[50]	2022	Ensemble model	0.974
[42]	2023	AdaBoost	0.99
		ANN	0.945
Proposed technique		PSO–ANN	0.954
		JSA–ANN	0.989

6. Sensitivity Analysis

For assessing the impact of all of the influential factors on flyrock, an analysis of sensitivity was conducted employing the cosine amplitude (CA) method (Equation (14)) introduced by Yang and Zhang [51]:

$$r_{ij} = \frac{\sum\limits_{k=1}^{l} g_{ik} \cdot g_{jk}}{\sqrt{\left(\sum\limits_{k=1}^{l} g_{ik}^2\right) \cdot \left(\sum\limits_{k=1}^{m} g_{jk}^2\right)}} \tag{14}$$

in which g_{ik} and g_{jk} indicate the inputs and output(s), respectively. k reveals the number of datasets. Noteworthy, a higher value of r_{ij} signifies inputs that matter most. Figure 14 shows the effect of each parameter on flyrock. The values of 0.993, 0.992, and 0.991 for the effectiveness of charge weight, powder factor, and hole angle demonstrated that this parameter had the highest effect on flyrock intensity; moreover, the burden with the r_{ij} value of 0.973 had the least effect on flyrock intensity. Furthermore, insignificant charge weight changes cause considerable flyrock changes.
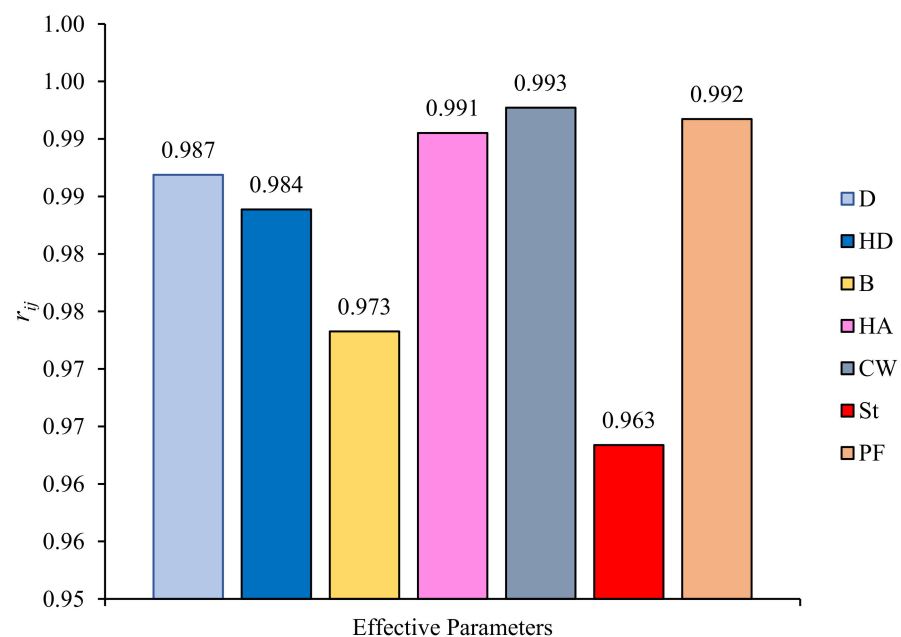
Figure 14. The effectiveness of considered variables on flyrock intensity.

7. Conclusions

This research focuses on the development of an innovative hybrid system for flyrock prediction in a quarry mines. To do this, the most influential variables on the flyrock distance-induced boulder blasting were identified from available literature and imported to the ANN model. The neurons' weights and biases were optimized by two optimization algorithms of PSO and JSA. The JSA–ANN model was first presented for estimating flyrock. For each ANN, PSO–ANN, and JSA–ANN model, the different models with various structures and swarm sizes were designed, and the evaluation indices of R^2, RMSE, and VAF were calculated for them.

To choose the best predictive model, a rating system was employed, and the model with the highest rate was introduced as the superior model. The evaluation of the achieved predictions indicated that both the PSO–ANN and JSA–ANN hybrid models are able to present precise results in estimating flyrock distance. However, the JSA–ANN model yields a higher accuracy prediction level and lower error. The R^2 values of (0.957, 0.972, and 0.995) and (0.945, 0.954, and 0.989) were determined to train and test the ANN, PSO–ANN and JSA–ANN predictive models, respectively. Moreover, the RMSE values of (7.392, 5.533, and 2.791) and (7.473, 7.751, and 2.896) were used to train and test the ANN, PSO–ANN and JSA–ANN models, respectively. These findings reveal the highest capability of the JSA–ANN hybrid model compared to the others.

It can be concluded that a hybrid JSA–ANN system is identified as the best predictive model to estimate flyrock distance if a predictive model with the highest accuracy and lowest error is required. It is worth noting that the results of sensitivity analysis indicated that the largest and smallest impact parameters on flyrock distance were charge weight and burden, respectively.

The current study has some limitations; thus, the following further examinations are suggested as possible next steps. Firstly, the data that was utilized may be extended to incorporate more full data with further blasting that was captured. Second, there is a desire to strengthen both the predictive and optimizing capabilities of the system. Third, since the number of data samples is relatively low, artificial data augmentation techniques can be used to increase the size and diversity of the dataset.

In light of the fact that the estimation and optimization models used in this investigation have room for development, it has been concluded that the utilization of novel approaches that enable the utilize hybrid combinations is the most effective method for improving both the estimation and optimization settings. Based on practical applications, the provided framework can be modified to apply to various sectors of engineering, particularly mining and building engineering. Nevertheless, the ensemble soft computing method can be used to boost the performance capacity of estimation objectives and enhance the accuracy level of soft computing approaches. These suggested techniques can be employed to conduct an analysis of safety data and locate possible dangers, blasting safety regions, and risks associated with blasting activities. The flyrock distance can be anticipated when the blasting activities begin in order to monitor for any possible problems or damages that could happen to the personnel, equipment, and residential area that is close to a safe area. If the anticipated outcomes are higher than those specified in the literature or standards, the blasting pattern or structure can be revised once again such that the anticipated flyrock values remain inside the safe limits that have been advised. In general, soft computing techniques can be applied to evaluate the data related to the environment and analyze the influence of mining activities on the surrounding ecosystem.

Author Contributions: Conceptualization, S.H., D.J.A. and E.T.M.; methodology, X.W., S.H. and D.J.A., software, X.W. and S.H., validation, X.W. and S.H., formal analysis, X.W. and S.H., data curation, D.J.A. writing—original draft preparation, X.W., S.H., D.J.A. and E.T.M., writing—review and editing, X.W., S.H., D.J.A. and E.T.M., supervision, D.J.A. and E.T.M. All authors have read and agreed to the published version of the manuscript.

Data Availability Statement: The data are available upon reasonable request.

Conflicts of Interest: The authors declare no conflict of interest.

References

1. Lundborg, N.; Persson, A.; Ladegaard-Pedersen, A.; Holmberg, R. Keeping the lid on flyrock in open-pit blasting. *Eng. Min. J.* **1975**, *176*, 95–100.
2. Gupta, R.N.; Bagchi, A.; Singh, B. Optimising drilling and blasting parameters to improve blasting efficiency. In *Status Report*; CBIP Rock Mech: New Delhi, India, 1988; pp. 185–206.
3. Hosseini, S.; Mousavi, A.; Monjezi, M.; Khandelwal, M. Mine-to-crusher policy: Planning of mine blasting patterns for environmentally friendly and optimum fragmentation using Monte Carlo simulation-based multi-objective grey wolf optimization approach. *Resour. Policy* **2022**, *79*, 103087. [CrossRef]
4. Hosseini, S.; Pourmirzaee, R.; Armaghani, D.J.; Sabri Sabri, M.M. Prediction of ground vibration due to mine blasting in a surface lead–zinc mine using machine learning ensemble techniques. *Sci. Rep.* **2023**, *13*, 6591. [CrossRef] [PubMed]
5. Hosseini, S.; Poormirzaee, R.; Hajihassani, M. An uncertainty hybrid model for risk assessment and prediction of blast-induced rock mass fragmentation. *Int. J. Rock Mech. Min. Sci.* **2022**, *160*, 105250. [CrossRef]
6. Hosseini, S.; Poormirzaee, R.; Hajihassani, M.; Kalatehjari, R. An ANN-Fuzzy Cognitive Map-Based Z-Number Theory to Predict Flyrock Induced by Blasting in Open-Pit Mines. *Rock Mech. Rock Eng.* **2022**, *55*, 4373–4390. [CrossRef]
7. Rezaei, M.; Monjezi, M.; Yazdian Varjani, A. Development of a fuzzy model to predict flyrock in surface mining. *Saf. Sci.* **2011**, *49*, 298–305. [CrossRef]
8. Bahrami, A.; Monjezi, M.; Goshtasbi, K.; Ghazvinian, A. Prediction of rock fragmentation due to blasting using artificial neural network. *Eng. Comput.* **2011**, *27*, 177–181. [CrossRef]
9. Monjezi, M.; Bahrami, A.; Varjani, A.Y.; Sayadi, A.R. Prediction and controlling of flyrock in blasting operation using artificial neural network. *Arab. J. Geosci.* **2011**, *4*, 421–425. [CrossRef]
10. Amini, H.; Gholami, R.; Monjezi, M.; Torabi, S.R.; Zadhesh, J. Evaluation of flyrock phenomenon due to blasting operation by support vector machine. *Neural Comput. Appl.* **2012**, *21*, 2077–2085. [CrossRef]
11. Zangoei, A.; Monjezi, M.; Armaghani, D.J.; Mehrdanesh, A.; Ahmadian, S. Prediction and optimization of flyrock and oversize boulder induced by mine blasting using artificial intelligence techniques. *Environ. Earth Sci.* **2022**, *81*, 359. [CrossRef]
12. Mohamad, E.T.; Armaghani, D.J.; Hajihassani, M.; Faizi, K.; Marto, A. A simulation approach to predict blasting-induced flyrock and size of thrown rocks. *Electron. J. Geotech. Eng.* **2013**, *18*, 365–374.
13. Trivedi, R.; Singh, T.N.; Raina, A.K. Prediction of blast-induced flyrock in Indian limestone mines using neural networks. *J. Rock Mech. Geotech. Eng.* **2014**, *6*, 447–454. [CrossRef]
14. Ghasemi, E.; Amini, H.; Ataei, M.; Khalokakaei, R. Application of artificial intelligence techniques for predicting the flyrock distance caused by blasting operation. *Arab. J. Geosci.* **2014**, *7*, 193–202. [CrossRef]
15. McKenzie, C.K. Flyrock range and fragment size prediction. In Proceedings of the 35th Annual Conference on Explosives and Blasting Technique, Denver, CO, USA, 8–11 February 2009; International Society of Explosives Engineers: Cleveland, OH, USA, 2009; Volume 2.
16. Ikram, R.M.A.; Ewees, A.A.; Parmar, K.S.; Yaseen, Z.M.; Shahid, S.; Kisi, O. The viability of extended marine predators algorithm-based artificial neural networks for streamflow prediction. *Appl. Soft. Comput.* **2022**, *131*, 109739. [CrossRef]
17. Ikram, R.M.A.; Dai, H.-L.; Al-Bahrani, M.; Mamlooki, M. Prediction of the FRP Reinforced Concrete Beam shear capacity by using ELM-CRFOA. *Measurement* **2022**, *205*, 112230. [CrossRef]
18. Ikram, R.M.A.; Jaafari, A.; Milan, S.G.; Kisi, O.; Heddam, S.; Zounemat-Kermani, M. Hybridized Adaptive Neuro-Fuzzy Inference System with Metaheuristic Algorithms for Modeling Monthly Pan Evaporation. *Water* **2022**, *14*, 3549. [CrossRef]
19. Ikram, R.M.A.; Goliatt, L.; Kisi, O.; Trajkovic, S.; Shahid, S. Covariance matrix adaptation evolution strategy for improving machine learning approaches in streamflow prediction. *Mathematics* **2022**, *10*, 2971. [CrossRef]
20. Ikram, R.M.A.; Dai, H.-L.; Ewees, A.A.; Shiri, J.; Kisi, O.; Zounemat-Kermani, M. Application of improved version of multi verse optimizer algorithm for modeling solar radiation. *Energy Rep.* **2022**, *8*, 12063–12080. [CrossRef]
21. Adnan, R.M.; Dai, H.-L.; Mostafa, R.R.; Islam, A.R.M.T.; Kisi, O.; Heddam, S.; Zounemat-Kermani, M. Modelling groundwater level fluctuations by ELM merged advanced metaheuristic algorithms using hydroclimatic data. *Geocarto Int.* **2023**, *38*, 2158951. [CrossRef]
22. He, B.; Armaghani, D.J.; Lai, S.H. Assessment of tunnel blasting-induced overbreak: A novel metaheuristic-based random forest approach. *Tunn. Undergr. Sp. Technol.* **2023**, *133*, 104979. [CrossRef]
23. Ghanizadeh, A.R.; Ghanizadeh, A.; Asteris, P.G.; Fakharian, P.; Armaghani, D.J. Developing bearing capacity model for geogrid-reinforced stone columns improved soft clay utilizing MARS-EBS hybrid method. *Transp. Geotech.* **2023**, *38*, 100906. [CrossRef]
24. Yang, H.; Wang, Z.; Song, K. A new hybrid grey wolf optimizer-feature weighted-multiple kernel-support vector regression technique to predict TBM performance. *Eng. Comput.* **2022**, *38*, 2469–2485. [CrossRef]
25. Yang, H.; Song, K.; Zhou, J. Automated Recognition Model of Geomechanical Information Based on Operational Data of Tunneling Boring Machines. *Rock Mech. Rock Eng.* **2022**, *55*, 1499–1516. [CrossRef]
26. Lundborg, N. *The Probability of Flyrock*; Swedish Detonic Research Foundation: Stockholm, Sweden, 1981.

27. Richard, A.B.; Moore, A.J. *Golden Pike Cut Back Fly Rock Control and Calibration of a Predictive Model*; Terrock Consulting Engineers Report; Kalgoorlie Consolidated Gold Mines: Subiaco, Australia, 2005; p. 37.

28. Monjezi, M.; Bahrami, A.; Yazdian Varjani, A. Simultaneous prediction of fragmentation and flyrock in blasting operation using artificial neural networks. *Int. J. Rock Mech. Min. Sci.* **2010**, *47*, 476–480. [CrossRef]

29. Monjezi, M.; Khoshalan, H.A.; Varjani, A.Y. Prediction of flyrock and backbreak in open pit blasting operation: A neuro-genetic approach. *Arab. J. Geosci.* **2012**, *5*, 441–448. [CrossRef]

30. Ghasemi, E.; Sari, M.; Ataei, M. Development of an empirical model for predicting the effects of controllable blasting parameters on flyrock distance in surface mines. *Int. J. Rock Mech. Min. Sci.* **2012**, *52*, 163–170. [CrossRef]

31. Monjezi, M.; Mehrdanesh, A.; Malek, A.; Khandelwal, M. Evaluation of effect of blast design parameters on flyrock using artificial neural networks. *Neural Comput. Appl.* **2013**, *23*, 349–356. [CrossRef]

32. Khandelwal, M.; Monjezi, M. Prediction of backbreak in open-pit blasting operations using the machine learning method. *Rock Mech. Rock Eng.* **2013**, *46*, 389–396. [CrossRef]

33. Trivedi, R.; Singh, T.N.; Gupta, N. Prediction of blast-induced flyrock in opencast mines using ANN and ANFIS. *Geotech. Geol. Eng.* **2015**, *33*, 875–891. [CrossRef]

34. Raina, A.K.; Murthy, V.M.S.R. Prediction of Flyrock Distance in Open Pit Blasting Using Surface Response Analysis. *Geotech. Geol. Eng.* **2016**, *34*, 15–28. [CrossRef]

35. Trivedi, R.; Singh, T.N.; Raina, A.K. Simultaneous prediction of blast-induced flyrock and fragmentation in opencast limestone mines using back propagation neural network. *Int. J. Min. Miner. Eng.* **2016**, *7*, 237–252. [CrossRef]

36. Rad, H.N.; Hasanipanah, M.; Rezaei, M.; Eghlim, A.L. Developing a least squares support vector machine for estimating the blast-induced flyrock. *Eng. Comput.* **2018**, *34*, 709–717. [CrossRef]

37. Hudaverdi, T.; Akyildiz, O. A new classification approach for prediction of flyrock throw in surface mines. *Bull. Eng. Geol. Environ.* **2019**, *78*, 177–187. [CrossRef]

38. Lu, X.; Hasanipanah, M.; Brindhadevi, K.; Bakhshandeh Amnieh, H.; Khalafi, S. ORELM: A Novel Machine Learning Approach for Prediction of Flyrock in Mine Blasting. *Nat. Resour. Res.* **2020**, *29*, 641–654. [CrossRef]

39. Hasanipanah, M.; Bakhshandeh Amnieh, H.; Amnieh, H.B. A fuzzy rule-based approach to address uncertainty in risk assessment and prediction of blast-induced Flyrock in a quarry. *Nat. Resour. Res.* **2020**, *29*, 669–689. [CrossRef]

40. Lawal, A.I.; Ojo, O.J.; Kim, M.; Kwon, S. Determination of blast-induced flyrock using a drone technology: A bibliometric overview with practical soft computing implementation. *Arab. J. Geosci.* **2022**, *15*, 1581. [CrossRef]

41. Ye, J.; He, X. A novel hybrid of ANFIS-based models using optimisation approaches to predict mine blast-induced flyrock. *Int. J. Environ. Sci. Technol.* **2023**, *20*, 3673–3686. [CrossRef]

42. Yari, M.; Armaghani, D.J.; Maraveas, C.; Ejlali, A.N.; Mohamad, E.T.; Asteris, P.G. Several Tree-Based Solutions for Predicting Flyrock Distance Due to Mine Blasting. *Appl. Sci.* **2023**, *13*, 1345. [CrossRef]

43. Chou, J.-S.; Truong, D.-N. A novel metaheuristic optimizer inspired by behavior of jellyfish in ocean. *Appl. Math. Comput.* **2021**, *389*, 125535. [CrossRef]

44. Chou, J.S.; Tjandrakusuma, S.; Liu, C.Y. Jellyfish Search-Optimized Deep Learning for Compressive Strength Prediction in Images of Ready-Mixed Concrete. *Comput. Intell. Neurosci.* **2022**, *2022*, 9541115. [CrossRef]

45. Kennedy, J.; Eberhart, R.C. Discrete binary version of the particle swarm algorithm. In Proceedings of the 1997 IEEE International Conference on Systems, Man, and Cybernetics. Computational Cybernetics and Simulation, Orlando, FL, USA, 12–15 October 1997; IEEE: New York, NY, USA, 1997. [CrossRef]

46. Bakhtavar, E.; Hosseini, S.; Hewage, K.; Sadiq, R. Green blasting policy: Simultaneous forecast of vertical and horizontal distribution of dust emissions using artificial causality-weighted neural network. *J. Clean. Prod.* **2021**, *283*, 124562. [CrossRef]

47. Hosseini, S.; Monjezi, M.; Bakhtavar, E.; Mousavi, A. Prediction of Dust Emission Due to Open Pit Mine Blasting Using a Hybrid Artificial Neural Network. *Nat. Resour. Res.* **2021**, *30*, 4773–4788. [CrossRef]

48. Hosseini, S.; Monjezi, M.; Bakhtavar, E. Minimization of blast-induced dust emission using gene-expression programming and grasshopper optimization algorithm: A smart mining solution based on blasting plan optimization. *Clean Technol. Environ. Policy* **2022**, *24*, 2313–2328. [CrossRef]

49. Zorlu, K.; Gokceoglu, C.; Ocakoglu, F.; Nefeslioglu, H.A.; Acikalin, S. Prediction of uniaxial compressive strength of sandstones using petrography-based models. *Eng. Geol.* **2008**, *96*, 141–158. [CrossRef]

50. Barkhordari, M.S.; Armaghani, D.J.; Fakharian, P. Ensemble machine learning models for prediction of flyrock due to quarry blasting. *Int. J. Environ. Sci. Technol.* **2022**, *19*, 8661–8676. [CrossRef]

51. Yang, Y.; Zhang, Q. A hierarchical analysis for rock engineering using artificial neural networks. *Rock Mech. Rock Eng.* **1997**, *30*, 207–222. [CrossRef]